

# Nanoscale

Accepted Manuscript



This is an *Accepted Manuscript*, which has been through the Royal Society of Chemistry peer review process and has been accepted for publication.

*Accepted Manuscripts* are published online shortly after acceptance, before technical editing, formatting and proof reading. Using this free service, authors can make their results available to the community, in citable form, before we publish the edited article. We will replace this *Accepted Manuscript* with the edited and formatted *Advance Article* as soon as it is available.

You can find more information about *Accepted Manuscripts* in the [Information for Authors](#).

Please note that technical editing may introduce minor changes to the text and/or graphics, which may alter content. The journal's standard [Terms & Conditions](#) and the [Ethical guidelines](#) still apply. In no event shall the Royal Society of Chemistry be held responsible for any errors or omissions in this *Accepted Manuscript* or any consequences arising from the use of any information it contains.

## ARTICLE

# Ultra-High-Density 3D DNA Arrays within Nanoporous Biocompatible Membranes for Single-Molecule-Level Detection and Purification of Circulating Nucleic Acids

Cite this: DOI: 10.1039/x0xx00000x

Received 00th January 2012,

Accepted 00th January 2012

DOI: 10.1039/x0xx00000x

[www.rsc.org/](http://www.rsc.org/)

M. Aramesh,<sup>\*a,d</sup> O. Shimoni,<sup>a,b</sup> K. Fox,<sup>a,c</sup> T.J. Karle,<sup>a</sup> A. Lohrmann,<sup>a</sup> K. Ostrikov,<sup>d,e</sup> S. Praver<sup>\*a</sup> and J. Cervenka<sup>a,f</sup>

Extracellular nucleic acids freely circulating in blood and other physiologic fluids are important biomarkers for non-invasive diagnostics and early detection of cancer and other diseases, yet difficult to detect because they exist in very low concentrations and large volumes. Here we demonstrate a new broad-range sensor platform for ultrasensitive and selective detection of circulating DNA down to the single-molecule level. The biosensor is based on a chemically functionalized nanoporous diamond-like carbon (DLC) coated alumina membrane. The few nanometer-thick, yet perfect and continuous DLC-coating confers the chemical stability and biocompatibility of the sensor, allowing its direct application in biological conditions. The selective detection is based on complementary hybridization of a fluorescently-tagged circulating cancer oncomarker (a 21-mer nucleic acid) with covalently immobilized DNA on the surface of the membrane. The captured DNAs are detected in the nanoporous structure of the sensor using confocal scanning laser microscopy. The flow-through membrane sensor demonstrates broad-range sensitivity, spanning from  $10^{15}$  molecules per  $\text{cm}^2$  down to single molecules, which is several orders of magnitude improvement compared to the flat DNA microarrays. Our study suggests that these flow-through type nanoporous sensors represent a new powerful platform for large volume sampling and ultrasensitive detection of different chemical biomarkers.

## Introduction

Extracellular nucleic acids, such as circulating DNAs and RNAs, are believed to have diverse and vital roles in genetic regulation and other physiological and pathological processes in plants and animals.<sup>1, 2</sup> Circulating nucleic acids are freely present in biological fluids, such as blood, plasma and urine. Recently, it has been discovered that circulating nucleic acids can serve as efficient blood-based biomarkers for early diagnosis of cancer in patients.<sup>3-5</sup> However, the concentrations of each type of circulating nucleic acids (such as microRNAs) expressed from either healthy or cancer cells in the blood plasma is relatively low ( $\sim 9,000$ - $134,000$  copies  $\mu\text{L}^{-1}$ ) and below the detection capability of the current detection technologies.<sup>3</sup> Therefore, for early cancer diagnosis and monitoring a response to therapy, highly-sensitive detection and capture of low concentrations of circulating nucleic acids are required. Although many scientific advances and technological improvements have been made in genetic analysis in recent

years, fast biosensing techniques for a small number of oligonucleotides achieving high precision and sensitivity with a single molecular level detection capability are still scarce.<sup>5-7</sup>

Nanotechnology offers an unprecedented opportunity to manipulate solid state materials for genetic detection and expression.<sup>8-10</sup> DNA arrays with a high density of oligonucleotides immobilized on flat surfaces have been widely used for genetic analysis and testing.<sup>11</sup> However, the sensitivity of these flat DNA microarrays is not sufficient for detecting low traces of circulating DNA that typically exist in biological fluids.<sup>3</sup> The fundamental requirement for such as a DNA/RNA sensor is to possess (i) a very large number of capture sites (high probability of detection), while (ii) being capable to detect single molecules (high sensitivity). Recently a large number of studies have been devoted to the design of new biosensing platforms that would enhance the performance of the DNA sensors.<sup>12-15</sup>

Nanopore-based sensing mechanisms are emerging as one of the most promising methods for detection of RNA/DNA fragments in a fluctuating background because they offer direct

real-time and label-free detection.<sup>16-19</sup> Such properties are highly desirable for non-invasive early cancer diagnosis. Nanopore sensing devices can be constructed from a single nanochannel or an array of nanopores arranged in a membrane. While a single nanopore has been found suitable for translocation and detection of a single DNA or RNA molecule,<sup>20-24</sup> nanoporous membranes offer a fast and high-throughput analysis of a large number of biological specimens. Nanoporous materials, due to the large surface area, can accommodate a much higher number of probes on their surface compared to flat substrates. Higher concentration of the probes on the sensor promises to provide a higher chance to capture the target circulating DNA molecules on the sensor surface. Additionally, the use of flow-through type membranes gives an opportunity to speed up the isolation and detection of the target molecules in large volumes via discriminatory size selection, filtration and separation.

There are many types of porous materials, such as silicon, silica, titania and alumina, which have been considered for biological and medical applications.<sup>20, 25-28</sup> Although these materials possess interesting features, such as easy and large-scale fabrication, narrow pore size distribution, mechanical robustness, tunable porous structure and controllable surface chemistry, their limited long-term chemical stability and biocompatibility remain an issue.<sup>29, 30</sup> Recently, we have developed a new method to protect the whole internal and external surface of nanoporous anodic aluminum oxide (AAO) membranes by using a conformal coating of diamond-like carbon (DLC).<sup>31</sup> The nanoporous DLC coated AAO membranes exhibit extremely good resistance to chemical and biological corrosion, similar to diamond, which is particularly important for both *in vitro* and *in vivo* applications. Additionally, the entire (internal and external) surface of these carbon-coated membranes offer an opportunity to be covalently functionalized with a variety of chemical groups to allow specific interaction with targeted molecules in sensing applications.<sup>32, 33</sup>

Here, we report the fabrication of multifunctional 3-dimensional DLC-AAO nanoporous membrane sensors for highly-sensitive and selective detection of nucleic acids. It is demonstrated that nanoporous flow-through carbon-coated membrane sensors exhibit much better sensor performance than planar devices due to their large specific surface area and efficient DNA capture in narrow nanochannels. In particular, we show the detection of cancer oncomarker RAK I, a common 21-mer biomarker in patients with prostate, breast and gynecological cancer.<sup>34</sup> Specifically, optical detection of hybridization with complementary DNA in nanoporous membranes down to the single-molecule level is demonstrated. The immobilized fluorescently tagged DNAs are detected inside the nanoporous membranes using depth profiling with confocal microscopy. The sensitivity and selectivity mechanism of DLC-AAO membrane sensors as a function of different concentrations of the analyte oncomarker is investigated. Additionally, a comparative analysis of the biocompatibility of the sensor materials with and without a DLC coating is performed.

## Results and Discussion

### Membrane sensor fabrication.

The AAO membranes used in this study have straight circular pore channels with a pore diameter of 150 nm and a

thickness of 100  $\mu\text{m}$ . Different pore shapes and sizes (10-450 nm) of AAO membranes can be produced by changing the parameters in the anodization process.<sup>35</sup> The surface of the AAO membranes was coated by ultrathin (2-5 nm) DLC films using a plasma-enhanced chemical-vapor deposition (CVD) method.<sup>36</sup> The details of the CVD fabrication method have been reported elsewhere.<sup>31</sup> The SEM and TEM images of the cross-section through the nanoporous DLC-AAO membranes are shown in Fig. 1. DLC forms a conformal coating over the entire internal and external surface of the nanoporous alumina structure. The DLC layer consists of a mixture of  $\text{sp}^3$  (65%) and  $\text{sp}^2$  (35%) bonded amorphous carbon, which provides an impermeable protecting layer to the membrane substrate. As a result, DLC coated membranes exhibit excellent resistance to different chemicals and harsh environments ( $1 < \text{pH} < 14$ ).

In the next fabrication step, the surface of the DLC-AAO membranes was chemically functionalized to induce specific moieties for selective capture and sensing of biomolecules. The schematic of the fabrication process of the carbon-coated membrane sensors is shown in Fig. 1. The surface of the DLC-AAO membrane sensor has been decorated with a probe single-strand DNA (21-mer) that is complementary to the target RAK I oligonucleotide. The surface functionalization was possible due to oxygen plasma treatment of membranes that introduced carboxylic groups to the surface. Carbodiimide chemistry has enabled to covalently attach single-strand DNA with amine group to carboxylic groups on the surface of membrane (Fig. 2). As carbodiimide chemistry is well acknowledged technique to attach various molecules, it can be robustly used to decorate the membrane surface with many other biomarkers. After the surface functionalization with probe DNAs, the membrane sensor can be used not only for selective capture of target DNA, but also for filtration and separation of larger biomolecules in physiological liquids.

### Working principle

Fig. 1 shows schematically, a concept of the working principle of the surface-functionalized membrane sensor for the detection and capture of circulating nucleic acids in blood. The selectivity of the sensor is provided by selective hybridization between the target DNA and the complementary DNA strands immobilized on the DLC surface. Large species and cells in blood are separated by the membrane and small molecules of blood plasma enter the nanopores and pass through the membrane. The captured target molecules in the membrane are detected using optical microscopy. Finally, the membrane filter is washed and cleaned for re-use.

Blood filtration and separation of blood plasma using nanoporous AAO membranes has been demonstrated in previous studies.<sup>22, 37</sup> The narrow pore size distribution and high uniformity of pores in the membranes have led to fast permeability and effective plasma separation by the membranes.<sup>38</sup> Penetration of cells and other big blood constituents into the membrane can be avoided by size-selective filtration by the nanopores ( $< 200$  nm), allowing passage of only smaller particles (such as protein and nucleic acids).<sup>22</sup>

The pre-filtration and separation process is expected to simplify the whole procedure of DNA detection from blood of patients into a single procedure. In this paper, we concentrate on proof-of-concept studies of the membrane sensor operation and response to different concentration of pure synthetic DNA solutions in water and blood. It is demonstrated that the nanoporous membrane sensors can significantly improve the sensitivity of DNA capture on the sensor surface compared to

the currently used flat sensors (Figs. 3 and S2 and Table S1 in Supplementary Information†). A combination of filtration and high sensitivity in a single membrane sensor also promises to provide higher probability of DNA capture when passing the DNA through the nanopores, which is ideal for the detection of very small concentration of cancer and other bio-markers in large volumes of blood or other physiological liquids.

The nanoporous membrane sensors have about three orders of magnitude higher surface area than flat surfaces used in the existing commercial DNA arrays.<sup>39</sup> The calculated total surface area of the membrane (with the top surface area of 1 cm<sup>2</sup>, thickness of 100 μm, pore diameter of 150 nm and porosity of ~10<sup>9</sup> pores cm<sup>-2</sup>) is approximately 1000 cm<sup>2</sup>.

Such a high specific surface area of the membrane sensors opens up an opportunity for the formation of high-density DNA array with the density of ~ 10<sup>15</sup> probes per cm<sup>2</sup> (for a 1 cm<sup>2</sup> macroscopic sample with a ~ 1000 cm<sup>2</sup> of total surface area).

### Hybridization

The target DNA (RAK I) is captured on the membrane sensor by a hybridization process based on hydrogen bonding with the probe DNAs covalently attached to the surface of the sensor. The hybridization experiment was performed using two different oligonucleotides to test selectivity of the binding mechanism. One was the target DNA, with exact complementary matches with the immobilized probe DNA, and the other one was a control DNA, which does not match with the immobilized probe DNA. The control and target DNAs were marked with a fluorescent dye (Alexa Fluor 647) to allow optical detection.

The dynamics of the DNA hybridization in the nanoporous membranes is shown in Fig. 3. The data correspond to the process of adsorption of labelled DNAs on the nanoporous membranes. Fig. 3 clearly shows that there is no detectable adsorption between the probes on the surface and non-complementary DNA. The adsorption profile of the target DNA as a function of concentration follows approximately the Langmuir adsorption model (Equation 1). In this simplified model it is assumed that diffusive molecules are attached and detached from the surface by constant rates using only a single binding energy.<sup>40, 41</sup> The Langmuir model is given by Equation 1:

$$A = \frac{K \times C}{1 + K \times C}, \quad (1)$$

where  $K$  is the equilibrium constant and  $C$  is the concentration of the solution and  $A$  is the fractional coverage of the surface. Hybridization is a complex phenomenon<sup>40, 41</sup> and an in-depth analysis is needed to fully understand the binding rates of the target to a probe DNA in a nanochannel. However, by comparing the hybridization in nanoporous membranes with normal flat DNA arrays of Glazer *et al.*,<sup>39</sup> one can clearly see a difference in the adsorption profile and saturation as a function of concentration (inset of Fig. 3). This result suggests that space confinement modifies the hybridization kinetics and dynamics in nanochannels compared to flat substrates.<sup>42</sup> The observed hybridization saturates at approximately 1000 pmol cm<sup>-2</sup> (~ 10<sup>15</sup> molecules) of target DNA on the surface. This is approximately 1000 times larger than the saturation concentration on flat substrates (~ 10<sup>12</sup> molecules in a 1 cm<sup>2</sup> sample).<sup>39</sup> Additionally, it is important to mention that the hybridization in the nanoporous structures is a relatively fast process. For example, equilibrium is achieved within 10 min in a 1 μM solution (Fig. S1†).

### Optical detection

The target molecules attached to the membrane sensor can be easily detected by fluorescence microscopy. Similar to any other optical immunosensors, the intensity of the fluorescent light is used as an indicator of the concentration of the captured molecules. Fig. 4a shows a microscopic image of the sample using a fluorescence illuminator. However, much higher sensitivity is achieved by using a confocal scanning laser microscope equipped with a 632.8 nm laser and a detector capable of detecting single photons. Confocal microscopy spectra of the samples with different concentrations of the captured DNA on their surface are shown in Fig. 4b. The intensity of the fluorescent emission exhibits a clear increase with the concentration of the analyte in the 3D nanoporous DNA arrays.

Figure 4c shows the response of the nanoporous sensor to varying target DNA concentration. The total intensity of the fluorescence has been estimated by integration of the surface under the spectrum and compared to the background signal. The background signal has been measured on a sample with zero DNA concentration on the surface. The sensors show a very low background signal, which is a crucial characteristic of a sensor with high sensitivity that is needed for detection of very low concentrations of target fluorescent DNA.

At high concentration of the target DNA (>1000 pmol cm<sup>-2</sup>), a saturation of all probe DNA binding sites on the sensor surface is achieved and the detected signal reaches a maximum. The saturation signal intensity from the nanoporous DLC-AAO array has been found dramatically higher than on flat diamond arrays prepared in the same way (Fig. S2†). This is due to the larger surface area of the nanoporous membrane compared to the flat sensors, which allows accommodation of 1000 times more DNA molecules on a 1 cm<sup>2</sup> sensor area.

The intensity at very low concentrations was measured at a single wavelength and spatially averaged over 100×100 μm<sup>2</sup> scan area to compensate for inhomogeneous distribution of the molecules across the sample. This method allows detecting hybridized fluorescent DNA in the sample down to individual DNA molecules. Thus, the detection sensitivity of the 3D nanoporous arrays spans from single molecules up to 10<sup>15</sup> molecules, which is several orders of magnitude better than the sensitivity of currently used flat DNA microarrays (~ 10<sup>10</sup> - 10<sup>12</sup> molecules cm<sup>-2</sup>).<sup>39</sup> Fig. 5a shows a 100×100 μm<sup>2</sup> scan of a nanoporous sensor with a low concentration of captured DNAs. At these very low concentrations the captured fluorescent DNA molecules are detected under the confocal microscope as bright spots, which can represent single and multiple DNA molecules. By careful statistical analysis of the emission properties of the bright spots we could determine that the majority of these spots belong to the single molecules. Based on this assumption that each bright spot represents a single molecule, the calculated density of the molecules in Fig. 5a, b is estimated to be ~ 10<sup>8</sup> and ~ 10<sup>6</sup> molecules per cm<sup>2</sup> of the sensor respectively.

Fig. 5b shows an example of single fluorescent DNA molecule detection by measuring the emission from a single fluorescent dye attached to a target DNA. In these images, the sizes of the bright spots are limited by the resolution of the microscope (to about 300 nm). It is confirmed that the emission of the spots match spectral properties of the fluorescent dyes with the expected emission at 670 nm (Fig. 5b). The single-molecule sensitivity was established by counting the emitted photons over the time using an avalanche photodiode (Fig. 5c). In agreement with previous single-molecule emission studies,<sup>43-45</sup> it is found that a single molecule exhibits an abrupt bleaching

characteristic unlike the ensemble of fluorescent molecules (for details see Supplementary Information Fig. S3†). If more than one emitter was present in the observed spot, either multiple discrete bleaching steps (two and three molecules) or a slow decay function (a larger number of molecules) have been observed. The result of these observations is summarized in Fig. 5c. Based on the statistical data, more than 50% of the observed single-spots correspond to single-molecule events.

To demonstrate that the hybridization process can also occur within the nanopores, depth profiling is performed using scanning confocal microscopy to allow detection of the single DNA molecules at different depths of the membrane. Fig. 5d shows a series of confocal images taken at 1  $\mu\text{m}$  step from the volume scans of the sample, where it can be seen the detection of the single DNA molecules at different depths of the membrane. The images confirm not only successful surface functionalization within the nanopores of membrane, but also the ability to filter complimentary DNA from solution.

Finally, it is worth of mentioning that the high detection ability originates predominantly from a low background signal (noise) of the DLC-AAO sensors. We were unable to observe single-molecules on pristine AAO membranes due the auto-fluorescence of AAO, which originates from the oxygen vacancies ( $F^+$  centers) in the material.<sup>46, 47</sup> The DLC plasma modification of AAO effectively passivates the fluorescent centers on the surface of AAO as shown in Fig. S4†.

### DNA in blood

To demonstrate the suitability of the DLC-AAO sensors for DNA detection in real biological conditions, we have performed DNA detection from the whole-blood (Fig. 4c). For this purpose, the synthetic target DNA was mixed with the whole-blood samples to obtain desired concentrations. The sensor response to the captured DNA in blood is almost identical to sensing in water (Fig. 4c and Fig. S5†). This is because the blood components do not interfere with the optical emission of the used molecular dye. The whole-blood has no realizable optical emission at the emission of Alexa Fluor 647 (Fig. S5†), when excited with  $\lambda_{\text{excitation}} = 630 \pm 5$  nm.

### Chemical Stability and Biocompatibility

Long-term stability of a biosensor is a crucial factor for its *in vitro* and *in vivo* applications. *In vivo* applications especially, require materials that exhibit excellent stability in the biological environment. AAO exhibits a poor chemical stability in slightly acidic or basic environments due to a gradual dissolution of alumina.<sup>48</sup> The  $\text{sp}^3$  bonded carbon materials, on the other hand, are well-known for their chemical resistivity. Table 1 presents results of chemical resistance of AAO and DLC-AAO membranes in comparison to diamond. DLC-AAO demonstrates excellent corrosion resistance against all tested chemicals with no signs of degradation, similar to diamond, whereas AAO has been completely etched in these acidic/basic conditions. This result clearly shows that the conformal coating of DLC layer is the key factor for the chemical stability of DLC-AAO membranes.

The strong corrosion resistivity of the membranes is advantageous for recovery/regeneration of the sensors. Recovery of used DLC-AAO sensors was achieved by cleaning the sensors with boiling NaOH. This treatment resulted in the removal of all biomolecules and DNA from the surface without affecting the surface chemistry of the membranes (Fig. S6†).

The reusability of the sensors was confirmed by reaching single-molecule detection on a recycled membrane (Fig. S7†).

Non-toxicity is another crucial factor of a good biosensor. The *in vitro* cytotoxicity test is a good measure of biocompatibility as it indicates how a biological tissue and cells will respond to the sensor material. To test the cytotoxicity, the samples were immersed in DMEM (Dulbecco's Modified Eagle's Medium), the extracts were collected and then exposed to mouse fibroblast (3T3 fibroblast) cells for 24 hours. This is a standard test, which mimics or even exaggerates the clinical conditions where the test material is used. Accordingly, when the AAO and DLC-AAO samples were immersed in the fibroblast cell culture, AAO shows moderate toxicity when compared to the control (tissue culture plastic). On the other hand, DLC-AAO exhibited clearly non-toxic behaviour (Fig. 6). This suggests good biocompatibility of the DLC-AAO membrane, and makes this membrane interesting for biological applications.

### Conclusions

We have demonstrated a successful implementation of flow-through nanoporous DLC-coated alumina membranes as stable, biocompatible and highly-sensitive sensors of circulating nucleic acids. We have investigated the capture of fluorescent cancer biomarkers (RAK I) in nanopores of the membrane sensors through hybridization with the complementary DNA using highly-sensitive optical detection methods.

The findings show that the 3D structure of the nanoporous sensors allows broad-range detection sensitivity with the ultimate single-molecule resolution, breaking down the detection limits of the current commercial flat DNA microarrays by several orders of magnitude. The large surface area of the membrane sensors allows accommodation of  $\sim 10^{15}$  of molecular probes (21-mers) in 1  $\text{cm}^2$  of a macroscopic sample, which dramatically enhances the detection capability of large concentrations of DNA in comparison to the flat arrays.

Additionally, we have studied the cytotoxicity and biostability of the used membrane sensors in various biological environments. The DLC-AAO membranes have been found to be biocompatible and exhibit excellent chemical and biological stability.

These results suggest that DLC-coated membranes represent a unique material platform for biosensing through DNA hybridization or another type of a selective biosensing strategy, which can be applied in different biological experiments, such as detection of DNA, antibodies and other important biomarkers. The possibility of a combination of size-selective filtration and ultrasensitive detection in a single sensor opens up a range of possibilities for detection of low quantity biomarkers in large sample volumes, which is in particular important for early diagnosis of cancer and other diseases.

### Methods

#### Fabrication of DLC-AAO membrane sensors

Free-standing whole-through AAO membranes were purchased from Synkera Technologies, Inc. The membranes were  $1 \times 1$   $\text{cm}^2$  squares with 150 nm pore size and 100  $\mu\text{m}$  thickness. The conformal coating of diamond-like carbon was

performed in a microwave plasma-enhanced chemical vapor deposition (MW-PECVD) chamber (Cyrannus system from Iplas GmbH) as described elsewhere.<sup>31</sup> The thickness of the coated carbon was 2–5 nm. Samples were oxidized and cleaned by a 30 second exposure to oxygen plasma with 50 W power followed by 10 min exposure to UV light. This short plasma exposure modifies only the surface atomic termination of the membranes by oxygen,<sup>31</sup> while the original structure of the membrane is maintained (Fig. S8†).

### Nucleic acids

All the PCR (polymerase chain reaction) synthesized oligonucleotides with an amine modification on the 3' end were purchased from GeneWorks. Target RAK I has a sequence of 5'-CCA GAC TGT GAG TTG CAA CAG-3' (MW = 6606).<sup>49</sup> Complementary DNA and non-complementary DNA (control) have the sequences of 5'-CTG TTG CAA CTC ACA GTC TGG-3' (MW = 6664) and 5'-TGT GAC ATC AGG AGG CTC AAA TC-3' (MW = 6101), respectively.

### Surface functionalization

The samples were immersed in 1 M 1-Ethyl-3-(3-dimethylaminopropyl)carbodiimide (EDC) solution for 15 min at room temperature to activate the carboxyl groups on the surface to form a reactive intermediate. The active intermediate then was reacted with amine group at the 3' end of a complementary oligonucleotide.

Specifically, 2 mL of probe DNA (complementary RAK I) (2  $\mu$ M in phosphate buffer saline (PBS)) was added to the membrane-EDC mixture at room temperature and kept mixing overnight. The samples were washed couple of times with Milli-Q water and gently dried with nitrogen flow for further analysis.

To calculate the concentrations, optical density of the probe DNA was measured before and after adsorption on the surface of the sensor using an optical adsorption method. The optical adsorption of the molecules ( $A_{260}$ ) was recorded at  $\lambda_{\max} = 260$  nm, using a Nanodrop (Thermo Scientific). The concentration of the probe DNA was reduced to 1.2  $\mu$ M after adsorption, which corresponds to adsorption of  $6.9 \times 10^{14}$  DNA molecules on the sensor.

### Fluorescent dye attachment

DNA labelling with fluorescent dye was carried out by incubating 524.6 nmol of DNA in 2 mL of PBS with a 5-fold molar excess of Alexa Fluor® 647 NHS Ester (Succinimidyl Ester) (Life Technologies). The reaction between the primary amine on the 3' end of DNA and NHS on the fluorescent dye was allowed to proceed for 2 h, after which the DNA was purified using a NAP-5 column (GE Healthcare).

### DNA detection and characterization

In the hybridization experiment, samples were immersed in a solution of target-DNA or non-complementary DNA with different concentrations (1 fM – 100  $\mu$ M). The reaction was performed at 45 °C and completed in 20 min. The concentrations of the solutions (> 0.1 nM) were measured before and after the hybridization using a Fluorometer (HORIBA MicroMax 384) equipped with Xenon lamp. The excitation wavelength was  $630 \pm 5$  nm and the emission spectrum was measured from 645 to 745 nm from a 100  $\mu$ L

quartz cuvette. The surface area of the spectrum was measured to calculate the concentration of the solution.

### DNA detection from blood

The fresh whole-blood samples were obtained from deceased pigs. The blood was filtered using a syringe filter with 10  $\mu$ m pore size to remove clots and other large-size impurities. Then the blood was diluted to  $\sim 10^6$  red-cells  $\text{mL}^{-1}$  using distilled water. The target DNA was mixed with the blood to obtain the desired DNA concentration. DNA detection in blood was performed in the same way as in water.

### Optical detection

Fluorescence images were taken using an upright microscope (Olympus) equipped with a halogen lamp, a 60 $\times$  objective lens, a red filter and a CCD camera. Custom built confocal scanning laser microscopy (CSLM) with a Helium–Neon laser (632.8 nm) was used for spectral acquisition, photon counting and single-molecule studies. Gas emission lines were removed with a narrow band filter centred at 632 nm. The laser light was coupled into a single mode fibre designed for 632 nm. The laser light was reflected from a dichroic beam splitter and was incident on the back of the infinity-corrected objective (100 $\times$  magnification and 0.95 numerical aperture). The diffraction limited spot excited fluorescence in the sample which was transmitted by the dichroic mirror. The laser light was blocked using a 632.8 nm notch filter. The light was then focused onto a multi-mode fibre (which acted as a pinhole) using an achromatic lens. The signal was then split into two channels using a multi-mode fibre splitter and detected using a SPCM-AQR-14 avalanche photodiode (APD), an Acton 2300i (30cm) spectrometer and a PicoHarp 300 correlator card. The samples were scanned in two dimensions by a computer-controlled piezoelectric device using LabVIEW. Optical spectra, photon counts and images were obtained with a laser power of 2  $\mu$ W (measured before the objective). The optical spectra were collected using an integration time of 1 sec.

### Biocompatibility tests

Cell viability tests (ISO 10993-12) were done by immersing clean membranes in DMEM (supplemented with 5% FBS) for 24 hours at 37°C, 5% CO<sub>2</sub>. Extracts were then collected and stored in 4°C until used for cell culture. Mouse fibroblasts (3T3 fibroblasts) were seeded in 100  $\mu$ L of fresh DMEM at 3200 cells per well of 96 wells and culture for 24 hours to obtain an established cell layer. The DMEM was then removed and replaced by 100  $\mu$ L of the extracts. The cells were then incubated for another 24 hours. At the end, 20  $\mu$ L of Celltiter Aqueous One solution (Promega) was added to each well of the plate and incubated (37°C, 5% CO<sub>2</sub>) for 4 hours. After 4 hours, optical densities (OD) of the wells were measured using a spectrophotometer at 490 nm. Background ODs at 690 nm of the wells were also measured. Cell numbers are proportional to the values of ODs. All experiments have 3 repeats.

### Acknowledgements

We acknowledge financial support from the University of Melbourne research and CSIRO top-up scholarships. The authors wish to acknowledge research facility and technical assistance from the Nanostructured Interfaces and Materials

Science Group (NIMS) led by Prof. F. Caruso at the department of Chemical and Biomolecular Engineering, the University of Melbourne. We thank Dr. P. A. Tran and D. Prakash Biswas at the Tissue Engineering Group at the department of Chemical and Biomolecular Engineering at the University of Melbourne, for cytotoxicity assay. We thank Dr. S. Rubanov and Dr. R. Curtain at microscopy unit of Bio21 institute for assistance with SEM and TEM imaging. Partial support from CSIRO Science Leadership Scheme and Australian Research Council is acknowledged. This research was supported under Australian Research Council's Discovery Projects funding scheme (project number DE120101100).

## Notes and references

<sup>a</sup> School of Physics, The University of Melbourne, Melbourne, Victoria 3010, Australia.

<sup>b</sup> School of Physics and Advanced Materials, University of Technology, Sydney, New South Wales 2007, Australia.

<sup>c</sup> School of Aerospace, Mechanical and Manufacturing Engineering, RMIT University, Carlton, VIC 3053, Australia.

<sup>d</sup> Plasma Nanoscience Laboratories, Commonwealth Scientific and Industrial Research Organisation (CSIRO), PO Box 218, Lindfield, NSW 2070, Australia.

<sup>e</sup> School of Chemistry, Physics, and Mechanical Engineering, Queensland University of Technology, Brisbane QLD 4000, Australia.

<sup>f</sup> Institute of Physics ASCR, v. v. i., Cukrovarnicka 10, Prague 6, Czech Republic.

\* Corresponding authors:

mrtz.aramesh@gmail.com, s.prawer@unimelb.edu.au

† Electronic Supplementary Information (ESI) available: Time dependent fluorescence intensity measurements, photoluminescence decay on flat and nanoporous arrays, fluorophore time traces and photoluminescence of AAO and DLC-AAO. See DOI: 10.1039/b000000x/

- 1 E. E. Creemers, A. J. Tijssen, Y. M. Pinto, *Circ. Res.*, 2012, **110**, 483.
- 2 P. Pinzani, F. Salviantini, M. Pazzagli, C. Orlando, *Methods*, 2010, **50**, 302.
- 3 P. S. Mitchell, R. K. Parkin, E. M. Kroh, B. R. Fritz, S. K. Wyman, E. L. Pogossova-Agadjanian, A. Peterson, J. Noteboom, K. C. O'Briant, A. Allen, D. W. Lin, N. Urban, C. W. Drescher, B. S. Knudsen, D. L. Stirewalt, R. Gentleman, R. L. Vessella, P. S. Nelson, D. B. Martin, M. Tewari, *Proc. Natl. Acad. Sci. USA*, 2008, **105**, 10513.
- 4 C. Bettegowda, M. Sausen, R. J. Leary, I. Kinde, Y. Wang, N. Agrawal, B. R. Bartlett, H. Wang, B. Lubber, R. M. Alani, E. S. Antonarakis, N. S. Azad, A. Bardelli, H. Brem, J. L. Cameron, C. C. Lee, L. A. Fecher, G. L. Gallia, P. Gibbs, D. Le, R. L. Giuntoli, M. Goggins, M. D. Hogarty, M. Holdhoff, S. M. Hong, Y. Jiao, H. H. Juhl, J. J. Kim, G. Siravegna, D. A. Laheru, C. Lauricella, M. Lim, E. J. Lipson, S. K. Marie, G. J. Netto, K. S. Oliner, A. Olivi, L. Olsson, G. J. Riggins, A. Sartore-Bianchi, K. Schmidt, M. Shih, S. M. Oba-

- Shinjo, S. Siena, D. Theodorescu, J. Tie, T. T. Harkins, S. Veronese, T. L. Wang, J. D. Weingart, C. L. Wolfgang, L. D. Wood, D. Xing, R. H. Hruban, J. Wu, P. J. Allen, C. M. Schmidt, M. A. Choti, V. E. Velculescu, K. W. Kinzler, B. Vogelstein, N. Papadopoulos, L. A. Diaz, Jr., *Sci. Transl. Med.*, 2014, **6**, 224ra24.
- 5 A. M. Newman, S. V. Bratman, J. To, J. F. Wynne, N. C. Eclov, L. A. Modlin, C. L. Liu, J. W. Neal, H. A. Wakelee, R. E. Merritt, J. B. Shrager, B. W. Loo, Jr., A. A. Alizadeh, M. Diehn, *Nat. Med.*, 2014, **20**, 548.
- 6 T. G. Drummond, M. G. Hill, J. K. Barton, *Nat. Biotechnol.*, 2003, **21**, 1192.
- 7 M. Schena, D. Shalon, R. W. Davis, P. O. Brown, *Science*, 1995, **270**, 467.
- 8 E. Stern, A. Vacic, N. K. Rajan, J. M. Criscione, J. Park, B. R. Ilic, D. J. Mooney, M. A. Reed, T. M. Fahmy, *Nat. Nanotechnol.*, 2010, **5**, 138.
- 9 V. Rai, H. C. Hapuarachchi, L. C. Ng, S. H. Soh, Y. S. Leo, C. S. Toh, *PLoS ONE*, 2012, **7**, DOI: 10.1371/journal.pone.0042346
- 10 R. T. Ranasinghe, T. Brown, *Chem. Commun.*, 2011, **47**, 3717.
- 11 L. Wang, P. C. Li, *Anal. Chim. Acta*, 2011, **687**, 12.
- 12 F. Lucarelli, S. Tombelli, M. Minunni, G. Marrazza, M. Mascini, *Anal. Chim. Acta*, 2008, **609**, 139.
- 13 L. Gao, C. Lian, Y. Zhou, L. Yan, Q. Li, C. Zhang, L. Chen, K. Chen, *Biosens. Bioelectron.*, 2014, **60**, 22.
- 14 T. Auger, J. Mathé, V. Viasnoff, G. Charron, J.-M. Di Meglio, L. Auvray, F. Montel, *Phys. Rev. Lett.*, 2014, **113**, 028302.
- 15 F. Matsumoto, K. Nishio, H. Masuda, *Advanced Materials*, 2004, **16**, 2105.
- 16 V. Kurz, E. M. Nelson, J. Shim and G. Timp, *ACS Nano*, 2013, **7**, 4057.
- 17 B. McNally, A. Singer, Z. Yu, Y. Sun, Z. Weng and A. Meller, *Nano Lett.*, 2010, **10**, 2237.
- 18 O. N. Assad, N. Di Fiori, A. H. Squires and A. Meller, *Nano Lett.*, 2015, **15**, 745.
- 19 G. A. T. Chansin, R. Mulero, J. Hong, M. J. Kim, A. J. deMello and J. B. Edel, *Nano Lett.*, 2007, **7**, 2901.
- 20 S. D. Alvarez, C. P. Li, C. E. Chiang, I. K. Schuller, M. J. Sailor, *ACS Nano*, 2009, **3**, 3301.
- 21 A. de la Escosura-Muñiz, W. Chunglok, W. Surareungchai, A. Merkoçi, *Biosens. Bioelectron.*, 2013, **40**, 24.
- 22 A. de la Escosura-Muniz, A. Merkoçi, *Small*, 2011, **7**, 675.
- 23 X. Wang, S. Smirnov, *ACS Nano*, 2009, **3**, 1004.
- 24 S. J. Li, J. Li, K. Wang, C. Wang, J. J. Xu, H. Y. Chen, X. H. Xia, Q. Huo, *ACS Nano*, 2010, **4**, 6417.
- 25 C. Pacholski, C. Yu, G. M. Miskelly, D. Godin, M. J. Sailor, *J. Am. Chem. Soc.*, 2006, **128**, 4250.
- 26 C. Pacholski, M. Sartor, M. J. Sailor, F. Cunin, G. M. Miskelly, *J. Am. Chem. Soc.*, 2005, **127**, 11636.
- 27 K. S. Mun, S. D. Alvarez, W. Y. Choi, M. J. Sailor, *ACS Nano*, 2010, **4**, 2070.
- 28 A. Thormann, N. Teuscher, M. Pfannmoller, U. Rothe, A. Heilmann, *Small*, 2007, **3**, 1032.
- 29 A. Debrassi, A. Ribbera, W. M. de Vos, T. Wennekes, H. Zuilhof, *Langmuir*, 2014, **30**, 1311.
- 30 K. E. La Flamme, K. C. Papat, L. Leoni, E. Markiewicz, T. J. La Tempa, B. B. Roman, C. A. Grimes, T. A. Desai, *Biomaterials*, 2007, **28**, 2638.

- 31 M. Aramesh, K. Fox, D. W. M. Lau, J. Fang, K. Ostrikov, S. Praver, J. Cervenka, *Carbon*, 2014, **75**, 452.
- 32 C. E. Nebel, B. Rezek, D. Shin, H. Uetsuka, N. Yang, *J. Phys. D: Appl. Phys.*, 2007, **40**, 6443.
- 33 C. E. Nebel, D. Shin, B. Rezek, N. Tokuda, H. Uetsuka, H. Watanabe, *J. R. Soc., Interface*, 2007, **4**, 439.
- 34 K. C. Kyriacou, F. Iacovou, A. Adamou, A. Hadjisavvas, E. M. Rakowicz-Szulczynska, *Exp. Mol. Pathol.*, 2000, **69**, 27.
- 35 W. Lee, S. J. Park, *Chem. Rev.*, 2014, **114**, 7487.
- 36 K. Ostrikov, E. C. Neyts, M. Meyyappan, *Adv. Phys.*, 2013, **62**, 113.
- 37 T. Kumeria, M. D. Kurkuri, K. R. Diener, L. Parkinson, D. Losic, , *Biosens. Bioelectron.*, 2012, **35**, 167.
- 38 A. C. Attaluri, Z. Huang, A. Belwalkar, W. Van Geertruyden, D. Gao, W. Misiulek, *ASAIJ*, 2009, **55**, 217.
- 39 M. Glazer, J. A. Fidanza, G. H. McGall, M. O. Trulson, J. E. Forman, A. Suseno, C. W. Frank, *Anal. Biochem.*, 2006, **358**, 225.
- 40 M. F. Hagan, A. K. Chakraborty, *J. Chem. Phys.*, 2004, **120**, 4958.
- 41 A. Halperin, A. Buhot, E. B. Zhulina, *J. Phys.: Condens. Matter*, 2006, **18**, S463.
- 42 M. I. Glazer, J. A. Fidanza, G. H. McGall, M. O. Trulson, J. E. Forman, C. W. Frank, *Biophys. J.*, 2007, **93**, 1661.
- 43 X. Michalet, S. Weiss, *C. R. Phys.*, 2002, **3**, 619.
- 44 E. M. Stennett, M. A. Ciuba, M. Levitus, *Chem. Soc. Rev.*, 2014, **43**, 1057.
- 45 M. Sauer, J. Hofkens, J. Enderlein, *Handbook of Fluorescence Spectroscopy and Imaging: From Single Molecules to Ensembles*. Wiley-VCH, 2011.
- 46 Z. Li, K. Huang, *J. Lumin.*, 2007, **127**, 435.
- 47 Y. Yamamoto, N. Baba, S. Tajima, *Nature*, 1981, **289**, 572.
- 48 C. W. Lee, H. S. Kang, Y. H. Chang, Y. M. Hahm, *Korean J. Chem. Eng.*, 2000, **17**, 266.
- 49 E. M. Rakowicz-Szulczynska, B. Jackson, A. M. Szulczynska, M. Smith, *Clin. Diagn. Lab. Immunol.*, 1998, **5**, 645.

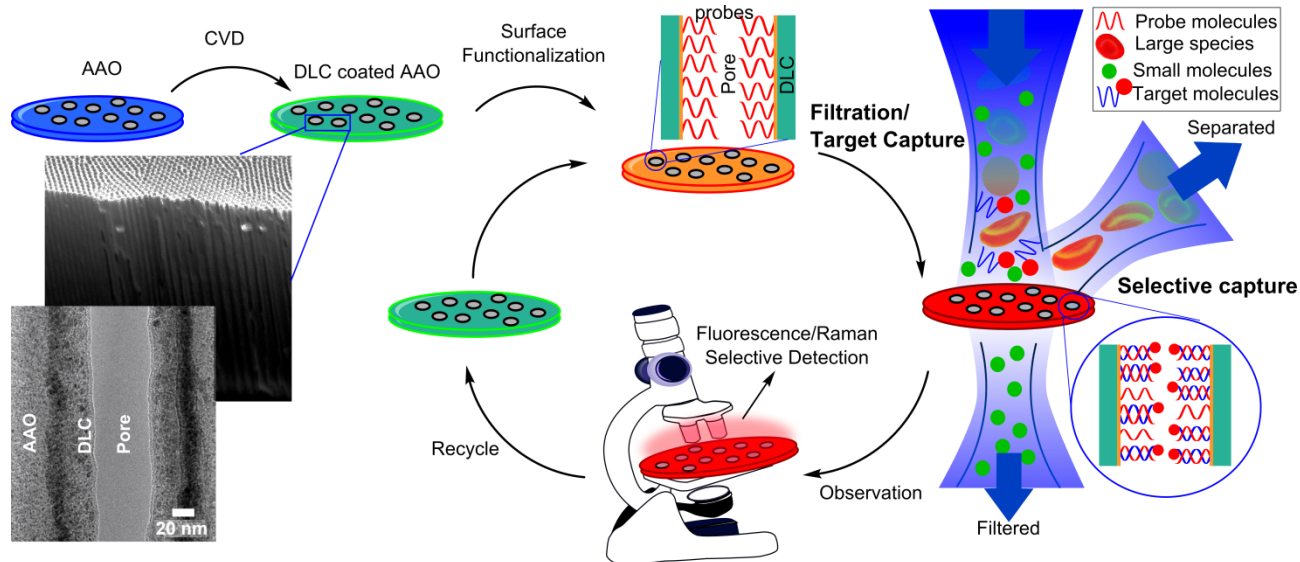


**Fig. 1.** DNA sensing technology using a diamond-like carbon coated AAO membrane filter. The schematics on the right show the sample fabrication and a concept of the working principle of the flow-through membrane sensor used for filtration and capture of target biomolecules in complex biological fluids. SEM and TEM images of a cross section through a DLC-AAO membrane are shown on the left.

## ARTICLE

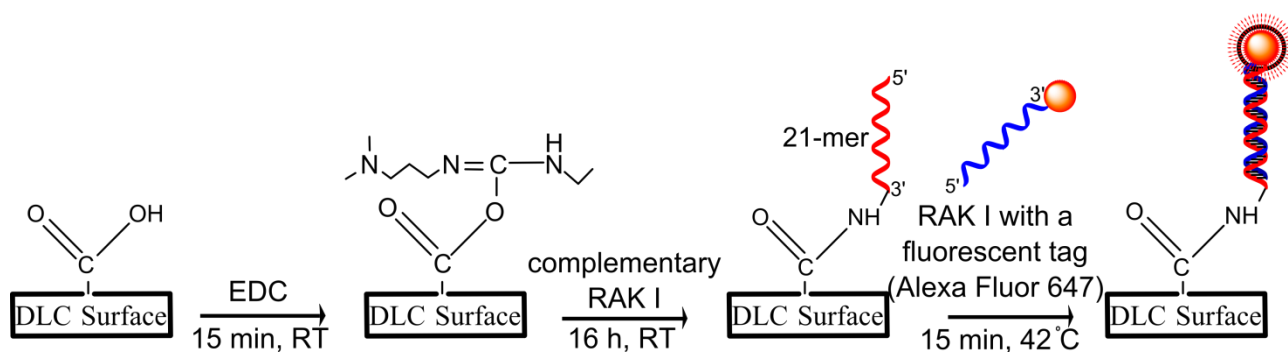


**Fig. 2.** Schematic presentation of chemical functionalization of DLC-AAO membranes using carbodiimide chemistry, DNA probe attachment, and fluorescently-tagged target capture through hybridization.

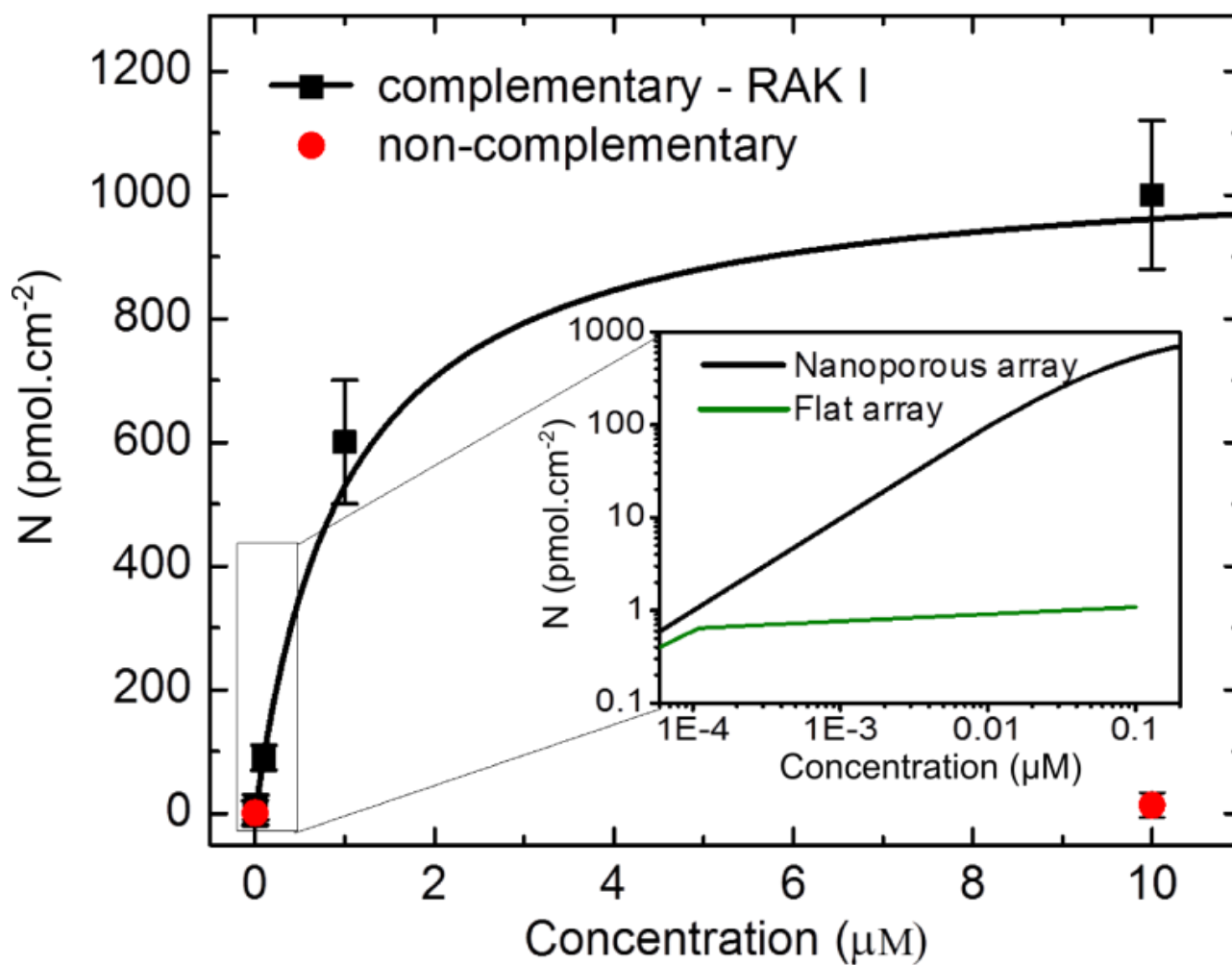


**Fig. 3.** Adsorbed density ( $N$ ) of complementary and non-complementary DNAs on DLC-AAO membrane sensors as a function of concentration. The line shows the Langmuir fit to the complementary adsorption. The inset shows comparison between DNA hybridization on flat substrate (from Glazer *et al.*)<sup>39</sup> and nanoporous DNA arrays. The nanoporous array has much higher surface area, therefore, it can accommodate 1000 times more DNA on its surface. Higher concentration of the probes on the sensor means higher chance for the target molecules to be captured.

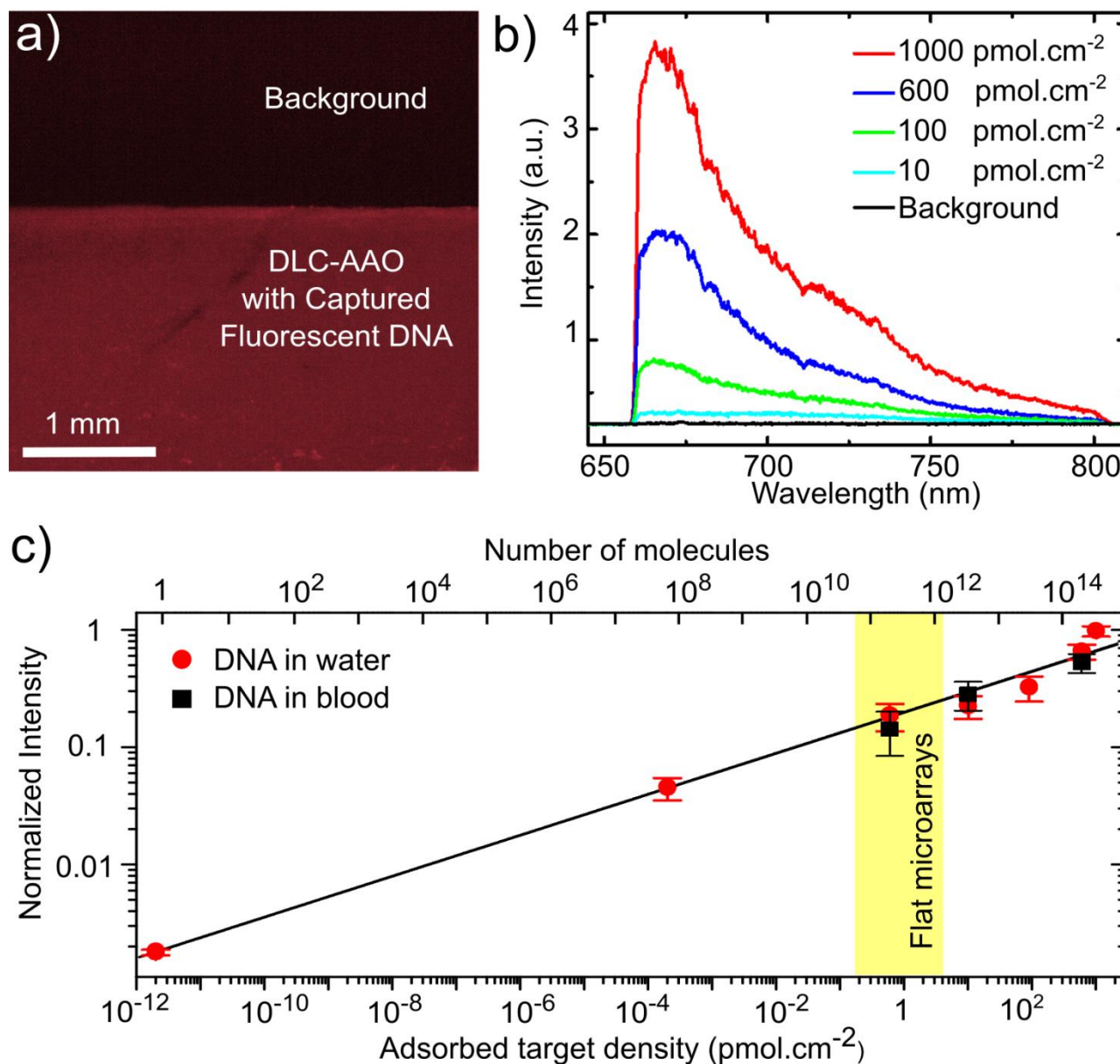


**Fig. 4.** a) A fluorescence microscopy image of DLC-AAO membrane saturated with captured fluorescent DNAs. b) Optical spectra of the samples with different adsorbed DNA concentrations on the surface obtained with confocal microscopy. c) Sensitivity analysis of the measured intensity as a function of the amount of captured molecules in 3D DNA nanoporous arrays in water and blood. The low density ( $10^{-12}$  -  $0.1 \text{ pmol cm}^{-2}$ ) data points were spatially averaged over a  $100 \times 100 \mu\text{m}^2$  scan area.

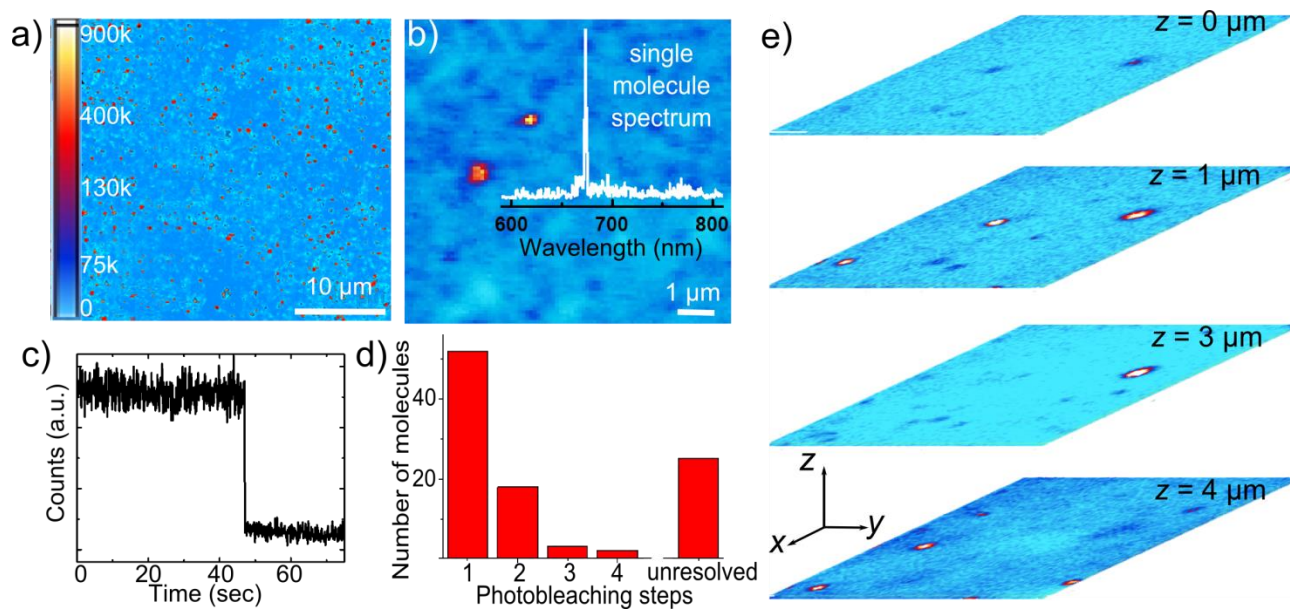


**Fig. 5.** a) A scanning confocal image of a  $100 \times 100 \mu\text{m}^2$  area of a DLC-AAO membrane with a low concentration of captured target DNA. b) A single-molecule event observed under the confocal microscope and the related spectrum. c) The photon counts from a single molecule before and after bleaching. d) Statistical analysis of photobleaching steps in single fluorophore spots. e) Observation of the single-molecules at different depths of the nanoporous membrane, and demonstration of 3D imaging of the 3D DNA array.

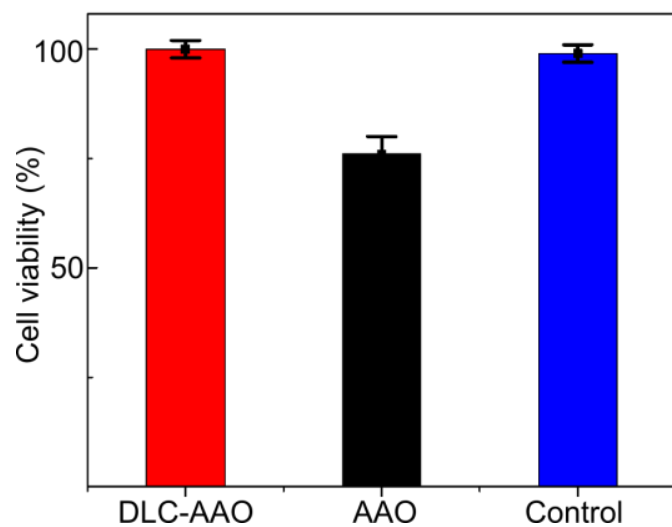


**Fig. 6.** Cytotoxicity of different materials (Cytotoxicity test – ISO 1099312). DLC-AAO and the control (tissue culture plastic) are non-toxic, while AAO exhibits moderate toxicity.

Chemical/Duration	pH	T (K)	AAO	DLC-AAO	Diamond
Saturated Potassium Hydroxide (KOH) / 24 hours	14	298	etched	resistant	resistant
Saturated Potassium Hydroxide (KOH) / 2 hours	14	353	etched	resistant	resistant
Phosphoric Acid (10% vol) / 12 hours	4	333	etched	resistant	resistant
Hydrofluoric Acid (HF 40% vol) / 72 hours	3.5	298	etched	resistant	resistant
Sulfuric Acid and Sodium Nitrate (1 mL H <sub>2</sub> SO <sub>4</sub> + 0.25 mg NaNO <sub>3</sub> ) / 1 hour boiling	1	473	etched	resistant	resistant

**Table 1.** Comparison of chemical resistance of AAO, DLC-AAO and diamond.